Crystal Plasticity Finite Element Simulations of Grain Interaction and Orientation Fragmentation during Plastic Deformation of BCC Metals

S.-J. Park[1], H.N. Han[1], K.H. Oh[2] , D. Raabe[3] and J.K. Kim[1]

[1] Technical Research Laboratories, POSCO, Pohang 790-785, Korea

[2] School of Materials Science & Engineering, College of Engineering, Seoul National University, Seoul 151-742, Korea

[3] Max-Planck-Institut für Eisenforschung, Max-Planck-Str. 1, 40237 Düsseldorf, Germany

Keywords: Grain interaction, Orientation fragmentation, Finite element simulation

Abstract. Deformation of a grain in polycrystalline metals is restricted or forced by deformation of neighbor grains during plastic deformation processes. It also gives influence to deformation of neighbor grains at the same time. Interaction between grains causes inhomogeneous local deformation and texture during plastic deformation. Prediction of inhomogeneous local deformation and texture is important in understanding of recrystallization texture. Taylor-type polycrystal models which have been employed in prediction of texture evolution can not count on grain interaction. In this work, a finite element simulation based on the crystal plasticity has been carried out to investigate the effect of grain interaction on local deformation and texture evolution. An artificially configured BCC bicrystal that consists of a crystal located at center and a surrounding neighbor crystal has been employed in plane strain compression simulation. Several pairs of specific orientations have been chosen for initial orientations of the bicrystal. Deformation and texture evolution of the center crystal in the bicrystal have been investigated changing the initial orientation of the surrounding crystal. The simulation results show that deformation and texture evolution near crystal boundary can be different from those at the center region of the crystal. Orientation fragmentation, which results in great lattice curvature is observed in a center grain with an initial metastable orientation. Simulation shows that a metastable crystal always breaks up during deformation and the grain interaction changes only the pattern of grain breakup.

Introduction

Heterogeneities in structure, stress and strain occur when polycrystalline metals undergo deformation. The heterogeneities in structure can be classified into heterogeneities within a grain and those involving several grains [1]. An important heterogeneity evolves when a grain is divided into zones of different crystallographic orientations. The divided grain usually shows banded structure that consists of mutually misoriented deformation bands separated by transition bands. The transition bands have sharp lattice curvature and high geometrically necessary dislocation density. An experimental measurement of the misorientation across a transition band showed a deviation of 30° over a distance of only 3μm [2]. These transition bands have been shown to be favoured sites for nucleation in recrystallization [3]. Transition bands are usually observed in grains with metastable orientations, such as cube components (001)[100] in FCC metals [4,5]. Strain heterogeneity within a grain of a polycrystal can also arise from the influence exercised by neighboring grains. Therefore evolution of heterogeneities in a grain during deformation could be a function of orientation of itself and orientations of neighboring grains. It has not been clear what is the main factor to give rise to orientation fragmentation. This work has been carried out to investigate the effects of grain interaction on orientation fragmentation tendency in BCC metals with selected sets of orientations.

Crystal Constitutive Model for the FE Simulations

The deformation behaviour of grains is determined by a crystal plasticity model that accounts for plastic deformation by crystallographic slip and for the rotation of the crystal lattice during deformation. The crystal kinematics follows those described by Asaro [6]. In this work, we used an implicit time-integration procedure for a crystal constitutive equation proposed by Kalidindi *et al.* [7]. The constitutive equation for the stress in each crystal is taken as

$$\boldsymbol{\sigma}^* = \mathbf{C}^{\mathrm{E}}[\mathbf{E}^*], \tag{1}$$

where

$$\mathbf{E}^* \equiv (1/2)\{\mathbf{F}^{*\mathrm{T}}\,\mathbf{F}^* - 1\} \text{ and } \boldsymbol{\sigma}^* \equiv \mathbf{F}^{*-1}\{(\det \mathbf{F}^*)\boldsymbol{\sigma}\}\mathbf{F}^{*-\mathrm{T}} \tag{2}$$

are elastic work conjugate strain and stress measure, respectively. $\mathbf{C}^{\mathrm{E}}$, $\boldsymbol{\sigma}$ and $\mathbf{F}^*$ are a fourth order elasticity tensor, the symmetric Cauchy stress tensor and an elastic deformation gradient, respectively. The shear rate $\dot{\gamma}^s$ on a slip system s is assumed to be related to the resolved shear stress on this system, τ^s, through a power law relation

$$\dot{\gamma}^s = \dot{\gamma}_0^s \left| \frac{\tau^s}{\tau_0^s} \right|^{1/m} \operatorname{sign}(\tau^s) \tag{3}$$

A crystal model including the constitutive equations has been implemented as a user material subroutine UMAT in the commercial finite element program ABAQUS [8]. It has been used in previous study to simulate deformation of polycrystalline materials [9,10]. In typical implicit finite element procedures, the principle of virtual work enforces both equilibrium and compatibility conditions.

Finite Element Simulations

For the current simulations, {110}<111>, {112}<111> and {123}<111> slip systems are considered. The rate sensitivity, m in equation (3) is set to be 0.02. A kind of bicrystal that consists of a crystal located at center and a surrounding neighbor crystal is used in simulation to investigate interaction between grains. Fig. 1 shows the initial finite element mesh, boundary conditions and configuration of bicrystal. The bicrystal is represented by 400 two-dimensional four-noded CPE4 elements [8]. Displacement boundary conditions are given to nodes on surfaces to make plane strain compression. Three different orientations are used for center crystal, and other three orientations are used for surrounding crystal. The Miller indices and Euler angles of these orientations are listed in Table 1.

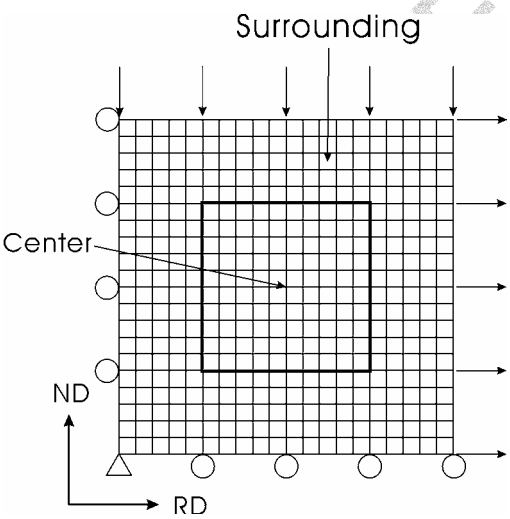

Fig. 1. Initial finite element mesh.

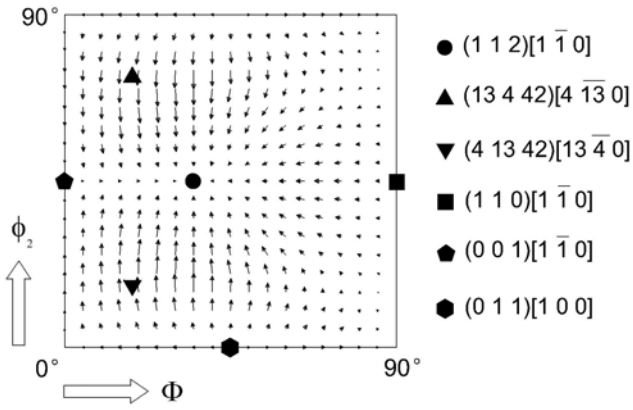

Fig. 2. Lattice rotation rates on the ϕ_1=0° section in Euler space for plane strain compression

The center and surrounding crystals have different orientation stability and strength according to orientations assigned to them. Fig. 2 shows the ϕ_1=0° ODF section representing lattice rotation rate field for plane strain compression. Among orientations for center crystal, $(11\,2)[1\,\bar{1}\,0]$ is stable, $(13\,4\,42)[4\,\overline{13}\,0]$ is unstable and $(0\,11)[1\,0\,0]$ is metastable, as can be seen in Fig. 2. For surrounding crystal, two orientations of $(0\,0\,1)[1\,\bar{1}\,0]$ and $(11\,0)[1\,\bar{1}\,0]$ which have symmetric configuration of slip systems relative to global coordinate system and one orientation of $(4\,13\,42)[13\,\bar{4}\,0]$ which has asymmetric configuration of slip systems are chosen. Between the two symmetric orientations, $(11\,0)[1\,\bar{1}\,0]$ orientation has a larger Taylor factor than $(0\,0\,1)[1\,\bar{1}\,0]$ orientation [2], which means that $(11\,0)[1\,\bar{1}\,0]$ orientation is harder in compression axis (ND) than $(0\,0\,1)[1\,\bar{1}\,0]$ orientation during plane strain compression.

Table 1. Miller indices and Euler angles for initial orientations of center and surrounding crystals.

Location	Normal Direction	Rolling Direction	Euler Angles		
			ϕ_1°	Φ°	ϕ_2°
Center	$(11\,2)$	$[1\,\bar{1}\,0]$	0	35	45
	$(13\,4\,42)$	$[4\,\overline{13}\,0]$	0	18	73
	$(0\,11)$	$[1\,0\,0]$	0	45	0
Surrounding	$(0\,0\,1)$	$[1\,\bar{1}\,0]$	0	0	45
	$(4\,13\,42)$	$[13\,\bar{4}\,0]$	0	18	17
	$(11\,0)$	$[1\,\bar{1}\,0]$	0	90	45

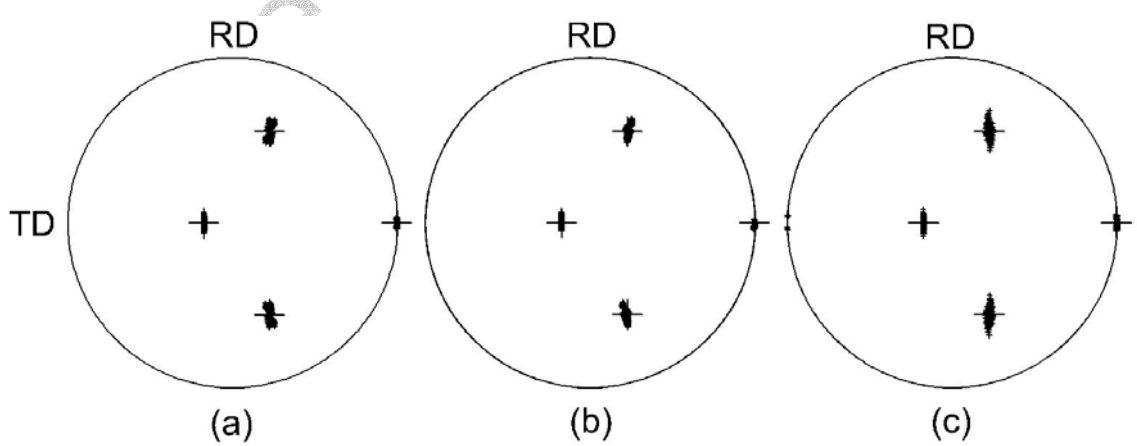

Fig. 3. (111) pole figures calculated by FEM for $(11\,2)[1\,\bar{1}\,0]$ initial center orientation with (a) $(0\,0\,1)[1\,\bar{1}\,0]$, (b) $(4\,13\,42)[13\,\bar{4}\,0]$ and (c) $(11\,0)[1\,\bar{1}\,0]$ surrounding orientations.

Total nine sets of center and surrounding orientation pair can be made up of all the six orientations for center or surrounding crystal, and each set is used for simulation of plane strain compression up to ε=-1.

Results and Discussion

Figs. 3 (a)-(c) show the (111) pole figures obtained from FEM simulation for initial center orientation of $(1\,1\,2)\,[1\,\bar{1}\,0]$ with $(0\,0\,1)\,[1\,\bar{1}\,0]$, $(4\,13\,42)\,[13\,\bar{4}\,0]$ and $(1\,1\,0)\,[1\,\bar{1}\,0]$ surrounding orientations, respectively. Big crosses represent the initial orientation and small crosses represent the final orientations. Though the final orientations show spread around the initial orientation, deviations from the initial orientation are less than 10°. It can be thought that this small deviation is originated from the stability of the initial $(1\,1\,2)\,[1\,\bar{1}\,0]$ orientation.

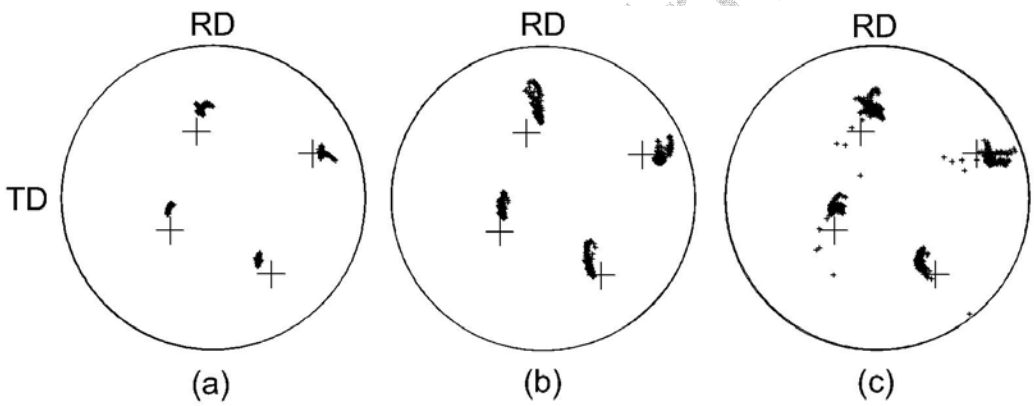

Fig. 4. (111) pole figures calculated by FEM for $(13\,4\,42)\,[4\,\overline{13}\,0]$ initial center orientation with (a) $(0\,0\,1)\,[1\,\bar{1}\,0]$, (b) $(4\,13\,42)\,[13\,\bar{4}\,0]$ and (c) $(1\,1\,0)\,[1\,\bar{1}\,0]$ surrounding orientations.

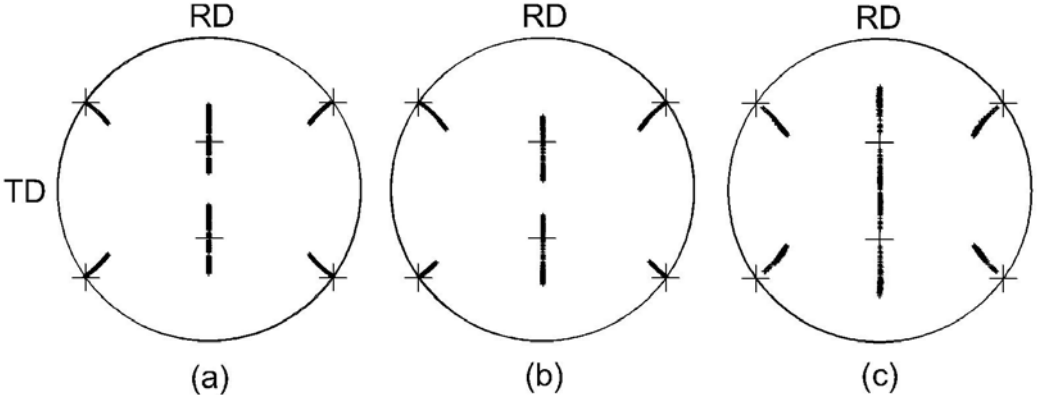

Fig. 5. (111) pole figures calculated by FEM for $(0\,1\,1)\,[1\,0\,0]$ initial center orientation with (a) $(0\,0\,1)\,[1\,\bar{1}\,0]$, (b) $(4\,13\,42)\,[13\,\bar{4}\,0]$ and (c) $(1\,1\,0)\,[1\,\bar{1}\,0]$ surrounding orientations.

Figs. 4 (a)-(c) show the (111) pole figures obtained from FEM simulation for initial center orientation of $(13\,4\,42)\,[4\,\bar{1}3\,0]$ with $(0\,0\,1)\,[1\,\bar{1}\,0]$, $(4\,13\,42)\,[13\,\bar{4}\,0]$ and $(1\,1\,0)\,[1\,\bar{1}\,0]$ surrounding orientations, respectively. The final orientations are rotated from the initial orientation due to the unstability of $(13\,4\,42)\,[4\,\bar{1}3\,0]$ orientation. Spread in the final orientations also can be observed and the deviations from an average orientation are within 15°. Some poles show a large deviation from the majority of final orientations in Fig. 4 (c), which shows a possibility of orientation fragmentation during deformation in initially non-metastable orientations. However, volume fraction of the region having the large deviation of orientation is very small in this case. Figs. 5 (a)-(c) show the (111) pole figures obtained from FEM simulation for initial center orientation of $(0\,1\,1)\,[1\,0\,0]$ with $(0\,0\,1)\,[1\,\bar{1}\,0]$, $(4\,13\,42)\,[13\,\bar{4}\,0]$ and $(1\,1\,0)\,[1\,\bar{1}\,0]$ surrounding orientations, respectively. The final orientations are split into orientations rotated clockwise and counter-clockwise around TD from the initial orientation. $(0\,1\,1)\,[1\,0\,0]$ is known as Goss orientation which rotates toward $(1\,1\,1)\,[2\,\bar{1}\,\bar{1}]$ and $(\bar{1}\,1\,1)\,[2\,1\,1]$ under plane strain compression. Deviations of the final orientations from the initial orientation are symmetric in Fig. 5 (a) and (c) and asymmetric in Fig. 5 (b) where the $(4\,13\,42)\,[13\,\bar{4}\,0]$ surrounding orientation has strong shear deformation behaviour during compression. The $(1\,1\,0)\,[1\,\bar{1}\,0]$ surrounding orientation makes the largest deviation of center orientation of about 30° from the initial orientation.

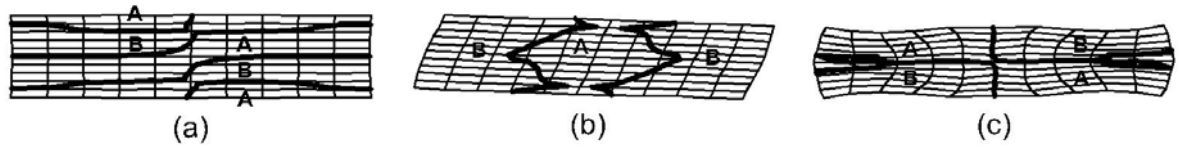

Fig. 6. Deformed meshes of center grain for $(0\,1\,1)\,[1\,0\,0]$ initial center orientation with (a) $(0\,0\,1)\,[1\,\bar{1}\,0]$, (b) $(4\,13\,42)\,[13\,\bar{4}\,0]$ and (c) $(1\,1\,0)\,[1\,\bar{1}\,0]$ surrounding orientations. A and B represent regions of clockwise and counter-clockwise lattice rotation around TD from the initial orientation, respectively.

Figs. 6 (a)-(c) show deformed meshes of center crystal for $(0\,1\,1)\,[1\,0\,0]$ initial center orientation with $(0\,0\,1)\,[1\,\bar{1}\,0]$, $(4\,13\,42)\,[13\,\bar{4}\,0]$ and $(1\,1\,0)\,[1\,\bar{1}\,0]$ surrounding orientations after plane strain compression, respectively. It can be noted that the deformed geometries of the three cases are different from each other due to interaction with different surrounding grains. A and B represent regions of clockwise and counter-clockwise lattice rotation around TD from the initial orientation, respectively, and can be regarded as deformation bands. Bold

lines are border of A and B regions where lattice maintains the initial $(0\,1\,1)[1\,0\,0]$ orientation and can be regarded as transition bands. Figs. 6 (a)-(c) show different patterns of orientation fragmentation from each other. This implies that interaction with neighbor grain has an influence on development of deformation bands. However, grain interaction does not change the orientation fragmentation tendency of metastable $(0\,1\,1)[1\,0\,0]$ orientation as can be seen in Figs. 5 and 6.

Summary

Plane strain compression of a BCC bicrystal has been simulated by a finite element method based on viscoplastic crystal plasticity. Nine pairs of center and surrounding orientation are chosen and used in calculations. Stable $(1\,1\,2)[1\,\bar{1}\,0]$, unstable $(13\,4\,42)[4\,\overline{13}\,0]$ and metastable $(0\,1\,1)[1\,0\,0]$ initial orientations show orientation spread after deformation. Orientation fragmented most in case of the metastable $(0\,1\,1)[1\,0\,0]$ initial orientation. Deformed geometry of center crystal and deformation bands evolution in initial $(0\,1\,1)[1\,0\,0]$ orientation show the influence of grain interaction on grain deformation and micro texture evolution. However, the orientation fragmentation tendency of metastable $(0\,1\,1)[1\,0\,0]$ orientation is not largely affected by neighbor grain orientations.

References

[1] J. Gil Sevillano, P. van Houtte and E. Aernoudt: Progress in Materials Science Vol. 25 (1981) pp. 69-412.

[2] I.L. Dillamore, P.L. Morris, C.J.E. Smith and W.B. Hutchinson: Proc. R. Soc. Lond. A. Vol. 329 (1972) pp. 405-420.

[3] J.L. Walter and E.F. Koch: Acta Metall. Vol. 11 (1963) pp. 923-938.

[4] Q. Liu, C. Maurice, J. Driver and N. Hansen: Metall. Mater. Trans. Vol. 29A (1998) pp. 2333-2344.

[5] F. Basson and J.H. Driver: Acta metall. Mater. Vol. 48 (2000) pp. 2101-2115.

[6] R.J. Asaro: Adv. appl. Mech. Vol. 23 (1983) pp. 1-115.

[7] S.R. Kalidindi, C.A. Bronkhorst and L. Anand: J. Mech. Phys. Solids Vol. 40 (1992) pp. 537-569.

[8] ABAQUS, Reference manuals, Hibbit, Karlsson and Sorensen, Inc., Pawtucket, RI, 1997.

[9] S.-J. Park, J.-H. Cho and K.H. Oh: ICOTOM-12 Montreal, Quebec, Canada, Aug. 9-13 (1999) pp. 700-705.

[10] J.-H. Cho, S.-J. Park, S.-H. Choi and K.H. Oh: ICOTOM-12 Montreal, Quebec, Canada, Aug. 9-13 (1999) pp. 587-592.

[11] D. Raabe, J. Boeslau: Proceedings 15th RISØ Int. Sympos. on Mat. Science: Numeri. Pred. of Def. Proc. and the Behaviour of Real Materials, eds.: S.I. Andersen, J.B. Bilde-Sorensen, T. Lorentzen, O.B. Pedersen and N.J. Sorensen. RISØ Nat. Lab, Roskilde, Denmark (1994) 481–486.

[12] D. Raabe, Z. Zhao, F. Roters: Proceedings of the 13th International Conference on Textures of Materials ICOTOM 13, 2002, Seoul, Korea, Trans Tech Publications, ed.: Dong Nyung Lee, Materials Science Forum, Vols. 408–412 (2002) 275–280.

[13] Z. Zhao, W. Mao, D. Raabe: Proceedings of the 13th International Conference on Textures of Materials ICOTOM 13, 2002, Seoul, Korea, Trans Tech Publications, ed.: Dong Nyung Lee, Materials Science Forum, Vols. 408–412 (2002) 281–286.

[14] S.-J. Park, H.N. Han, K.H. Oh, D. Raabe, J.K. Kim: Proceedings of the 13th International Conference on Textures of Materials ICOTOM 13, 2002, Seoul, Korea, Trans Tech Publications, ed.: Dong Nyung Lee, Materials Science Forum, Vols. 408–412 (2002) 371–376.

[15] D. Raabe: physica status solidi (b) 181 (1994) 291–299

[16] D. Raabe, Z. Zhao, S.–J. Park, F. Roters: Acta Materialia 50 (2002) 421–440